ACS OMEGA

http://pubs.acs.org/journal/acsodf

Article

Nanoparticle-Based Photodynamic Inhibition of *Candida albicans* Biofilms with Interfering Quorum Sensing

Na Tang,[§] Shenghao Yuan,[§] Yuxuan Luo,[§] An-Jun Wang, Kang Sun, Ning-Ning Liu,* and Ke Tao*

Cite This: *ACS Omega* 2023, 8, 4357−4368

Read Online

ACCESS | Metrics & More | Article Recommendations

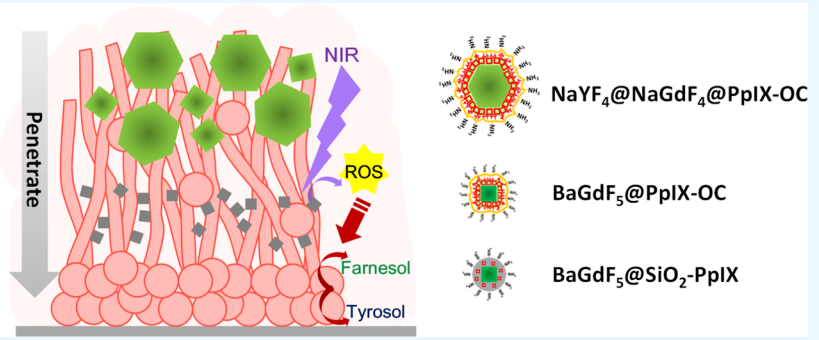

ABSTRACT: Biofilm formation is a critical event in the pathogenesis and virulence of fungal infections caused by *Candida albicans*, giving rise to about a 1000-fold increase in the resistance to antifungal agents. Although photodynamic treatment (PDT) has been excellently implicated in bacterial infections, studies on its potential against fungal infection through the clearance of fungal biofilm formation remain at its infancy stage. Here, we have designed photodynamic nanoparticles with different sizes, modifications, and the ability of generating reactive oxygen species (ROS) to examine their effects on inhibiting biofilm formation and destructing mature biofilms of *C. albicans*. We found that the nanoparticles modified with oligo-chitosan exhibited a better binding efficiency for planktonic cells, leading to stronger inhibitory efficacy of the filamentation and the early-stage biofilm formation. However, for mature biofilms, the nanoparticles with the smallest size (∼15 nm) showed the fastest penetration speed and a pronounced destructing effect albeit conferring the lowest ROS-producing capability. The inhibitory effect of photodynamic nanoparticles was dependent on the disruption of fungal quorum sensing (QS) by the upregulation of QS molecules, farnesol and tyrosol, mediated through the upregulation of ARO 8 and DPP 3 expression. Our findings provide a powerful strategy of nanoparticulate PDT to combat fungal infections through the inhibition of both hyphal and biofilm formation by disrupting QS.

1. INTRODUCTION

As the major opportunistic human fungal pathogen,[1] *Candida albicans* poses a significant threat to human health, having caused a high mortality of over 50% in the past decades.[2,3] Biofilms are dominant contributors to *C. albicans* infection. They can protect the fungal pathogens against host immune defense and thus promote fungal pathogenesis. Consequently, the classical therapies, by removing infected lesions or administrating antifungal agents, can hardly eliminate the fungal pathogens, and a high drug dosage usually causes severe side-effects and resistance.[4,5] Once the biofilm-protected pathogens survive the antifungal killing, they could be the origin of re-infection.[6,7] Currently, "Lock therapy" is the primary clinical strategy with partial success in preventing biofilm formation on medical devices. This approach diffuses a high concentration of antifungal agents into the devices, like catheter lumens. However, it has limitations in avoiding systemic toxicity since it was only effective before contacting patients.[8] Due to the lack of efficient anti-biofilm strategies, the mortality of fungal infections remains above 30% after treatment.[3,9]

Photodynamic treatment (PDT) that excites non-toxic photosensitizers (PSs) to generate highly oxidative reactive oxygen species (ROS) has been introduced as a promising method to prevent cancer,[10] kill pathogens,[11] and inactivate viruses.[12] The generated ROS can damage a series of lipids, proteins, and DNA molecules existing not only in individual cellular structures but also in biofilms.[13] Previous studies had assessed the potential of PDT in fungal biofilm inhibition by employing the molecular forms of PSs.[14] For example, Rosseti

Received: December 5, 2022
Accepted: January 17, 2023
Published: January 17, 2023

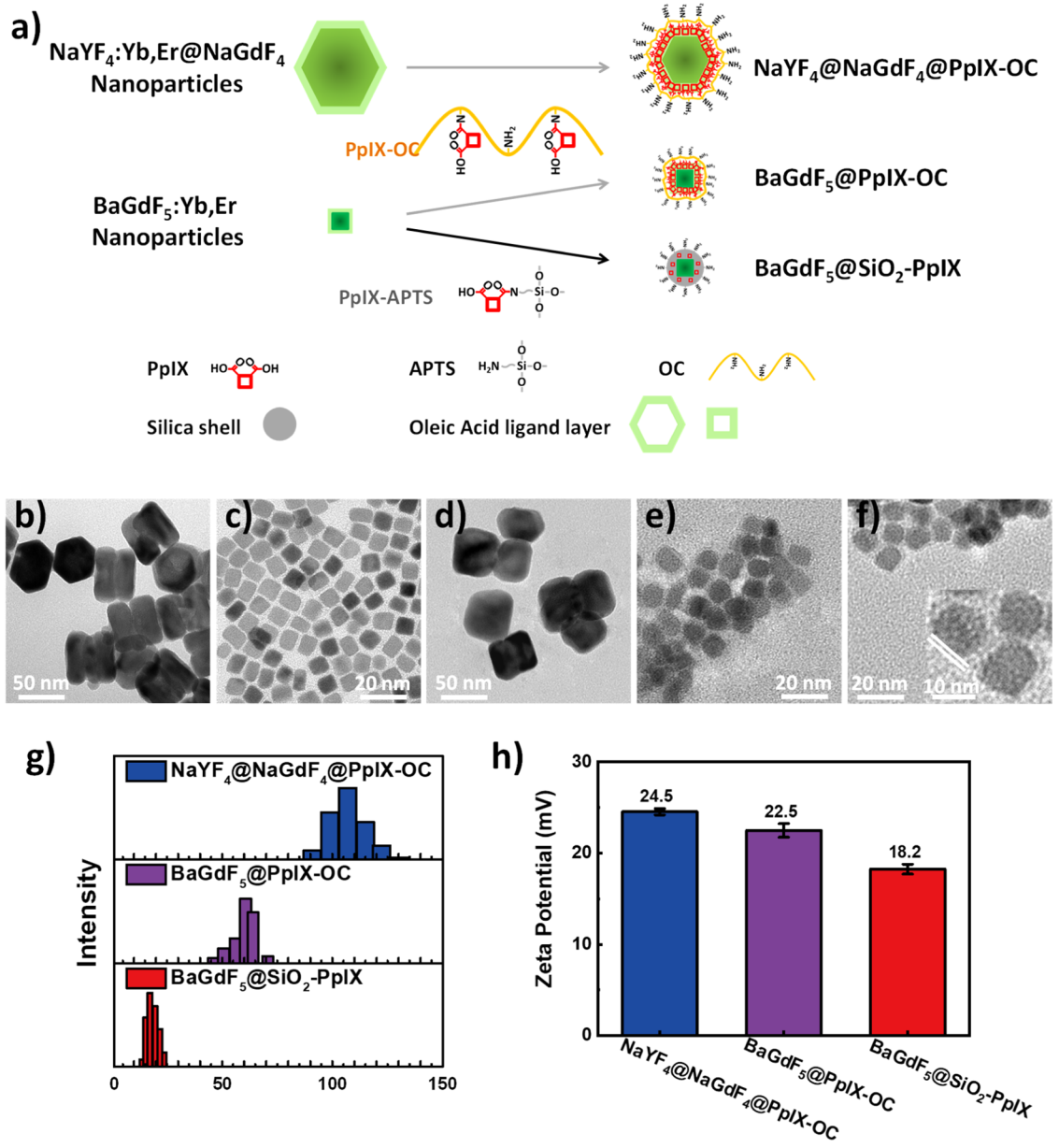

Figure 1. (a) Schematic illustration of the three kinds of photodynamic nanoparticles. TEM images of (b) $NaYF_4$:20%Yb,0.2%Er@$NaGdF_4$, (c) $BaGdF_5$:20%Yb,0.2%Er, (d) $NaYF_4$@$NaGdF_4$@PpIX-OC, (e) $BaGdF_5$@PpIX-OC, and (f) $BaGdF_5$@SiO_2-PpIX. (g) Hydrodynamic radius and (h) surface charges of $NaYF_4$@$NaGdF_4$@PpIX-OC, $BaGdF_5$@PpIX-OC, and $BaGdF_5$@SiO_2-PpIX, respectively.

et al. used 0.1 mg/mL toluidine blue as the PS, achieving a 60% efficiency to block *C. albicans* biofilm formation.[15] In contrast, Černáková et al. compared the susceptibility of planktonic *C. albicans* cells and the mature biofilm to PDT with methylene blue (MB) as the PS. The MIC50 (minimal inhibitory concentration reducing the biofilm mass to 50%) of MB was about 100 times that of the planktonic cells.[16] However, the effect of PDT with erythrosine as a PS was unsatisfactory as there was only a slight reduction of ∼0.15 (log_{10}) CFU·mL^{-1} in the clearance of the *C. albicans* biofilm, in contrast to about 3.45 (log_{10}) CFU·mL^{-1} for the planktonic cells.[17,18] These studies were explained by the assumption that the PSs must locate inside the biofilm because of the short half-life and limited effective radius of ROS. However, the ability of PSs to adhere to or penetrate into certain biofilms is largely unknown and might be inconsistent across different molecules.[18−20] Thus, these results raised a big challenge of choosing appropriate PDT sensitizers for combating fungal biofilms.

The development of nanotechnology provides pivotal carriers that can concentrate PS molecules at the targeted site.[11,21,22] Currently, significant achievements have been made in attacking bacterial biofilms by nanoparticle-based PDT.[11,22] However, fungi are markedly different from bacteria. For example, the cell wall structure of the eukaryotic fungal cells is much more complicated, resulting in distinct components of the extracellular matrix (ECM) of the biofilms.[5] In contrast to the monomorphic bacteria, *C. albicans* are more complex with the forms of yeast, pseudohyphae, and hyphae. At the early stage of biofilm formation, the yeast cells adhere to the substance and then start to transform to hyphae by initiating filaments, which will invade the surrounding tissue and increase the pro-inflammatory response.[23] Moreover, the regulatory factors within the fungal biofilm are different.[24,25]

https://doi.org/10.1021/acsomega.2c07740
ACS Omega 2023, 8, 4357−4368

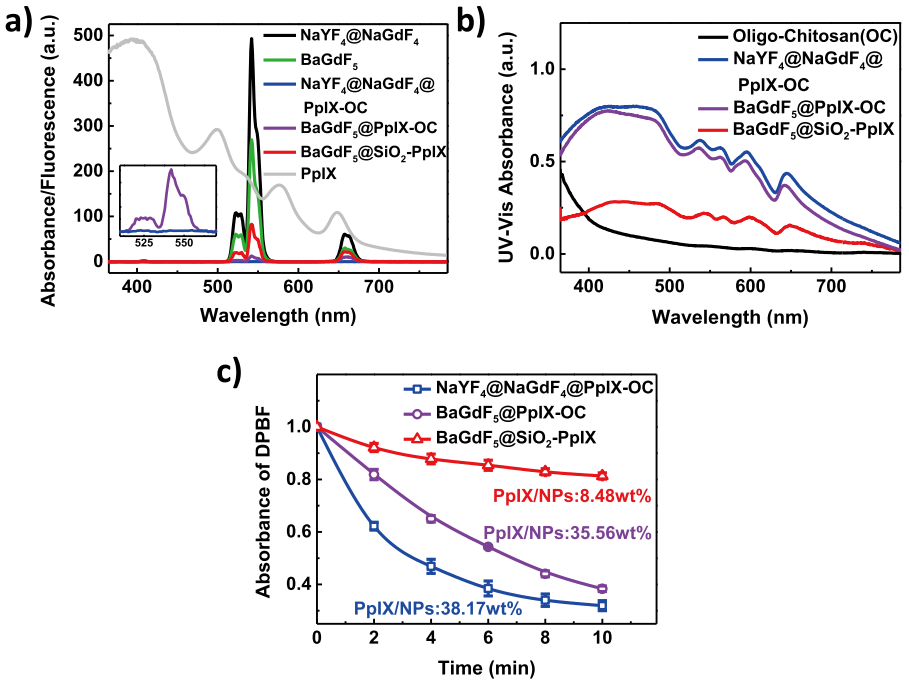

Figure 2. (a) UV−vis absorption spectrum of PpIX and the fluorescence spectra of two UCN cores and three kinds of PDT nanoparticles. (b) UV−vis absorption of an OC solution, $NaYF_4$@$NaGdF_4$@PpIX-OC, $BaGdF_5$@PpIX-OC, and $BaGdF_5$@SiO_2-PpIX. (c) ROS generation of different nanoparticles indicated by the decay of DPBF and the calculated weight ratio of the PpIX payload.

For example, the bacterial biofilm has a porous channel within the inner space, and nanoparticles with a size of less than 100 nm could penetrate.[26] Thus, for bacteria, nanoparticles with specific modifications could target the biofilm matrix and the outer membrane or even the intracellular structure of the protected pathogens.[13] In contrast, fungal biofilms are very dense, which might prevent the penetration of nanoparticles. Therefore, how the nanoparticles-fungal biofilm interacts and how ROS attacks biofilm formation merit further exploration.

In this study, we employ upconversion nanoparticles (UCNs) as a functional nanocarrier to load protoporphyrin IX (PpIX), forming efficient nanoparticulate sensitizers. UCNs can absorb near-infrared light (NIR) and emit visible ones so that the loaded PS can be stimulated by an NIR laser. This feature potentially expands the photodynamic method to treating deep-seated infectious.[27] Thus, $NaYF_4$@$NaGdF_4$ and $BaGdF_5$ nanoparticles were synthesized with variant sizes (about 50 and 10 nm respectively), providing different intensities of upconverting fluorescence. We further introduced oligo-chitosan (OC) and silica shell to modify UCNs, respectively, to obtain different hydrodynamic sizes and ROS generating efficiencies. In total, we have designed three PDT nanoparticles, namely, $NaYF_4$@$NaGdF_4$@PpIX-OC, $BaGdF_5$@PpIX-OC, and $BaGdF_5$@SiO_2-PpIX. With the adjustment of modification molecules and hydrodynamic size, we were enabled to evaluate the influence on their interactions with planktonic fungal cells and biofilms at different stages. Meanwhile, the variance of ROS production could help us in evaluating how the ROS damage the planktonic cells and biofilms. We further uncovered the mechanism of PDT through the interfering quorum sensing (QS) pathway by regulating the expression of both farnesol and tyrosol. These findings revealed the potential of PDT nanoparticles for future antifungal development.

2. RESULTS AND DISCUSSION

2.1. Preparation and Characterization of Photodynamic Nanoparticles. To examine the antifungal effect of nanoparticles, we sought three PDT nanoparticles from two kinds of UCNs with different sizes and modifications, as shown in Figure 1a. For the UCNs, $NaYF_4$:Yb,Er@$NaGdF_4$ and $BaGdF_5$:Yb,Er were synthesized, in which $NaYF_4$:Yb,Er@$NaGdF_4$ had a core−shell structure with a size of 50 nm, and the size of $BaGdF_5$:Yb,Er nanoparticles was controlled as 10 nm. One method for the surface modification was covalently conjugating PpIX with OC, followed by directly assembling it onto the surface of UCNs. OC was chosen due to its ability to embed into the fungal cell wall structure. On the other hand, PpIX and (3-aminopropyl)triethoxysilane (APTS) were covalently connected as a silane, which was then condensed onto $BaGdF_5$:Yb,Er nanoparticles. By this way, a thin hydrophilic silica layer could be formed with plentiful amino groups on the UCNs surface, resulting in a positive charge.[28] The three PDT nanoparticles were denoted as $NaYF_4$@$NaGdF_4$@PpIX-OC, $BaGdF_5$@PpIX-OC, and $BaGdF_5$@SiO_2-PpIX, respectively. As shown in the transmission electron microscopy (TEM) images in Figure 1b−f, two kinds of inorganic cores exhibiting higher contrast showed different sizes (50 and 10 nm, respectively), and there was a thin shell of around 2 nm for the $BaGdF_5$@SiO_2-PpIX nanoparticles. Meanwhile, the hydrodynamic radii of $NaYF_4$@$NaGdF_4$@PpIX-OC, $BaGdF_5$@PpIX-OC, and $BaGdF_5$@SiO_2-PpIX were about 110, 50, and 15 nm, respectively, when they were dispersed in distilled water (as shown in Figure 1g). The different hydrodynamic radii should be ascribed to not only the inorganic core but also the coating layer by which the molecular chain of PpIX-OC can spread into the solvent, whereas the silica layer was solid. The surface charge slightly decreased in the sequence of $NaYF_4$@$NaGdF_4$@PpIX-OC, $BaGdF_5$@PpIX-OC, and $BaGdF_5$@

https://doi.org/10.1021/acsomega.2c07740
ACS Omega 2023, 8, 4357−4368

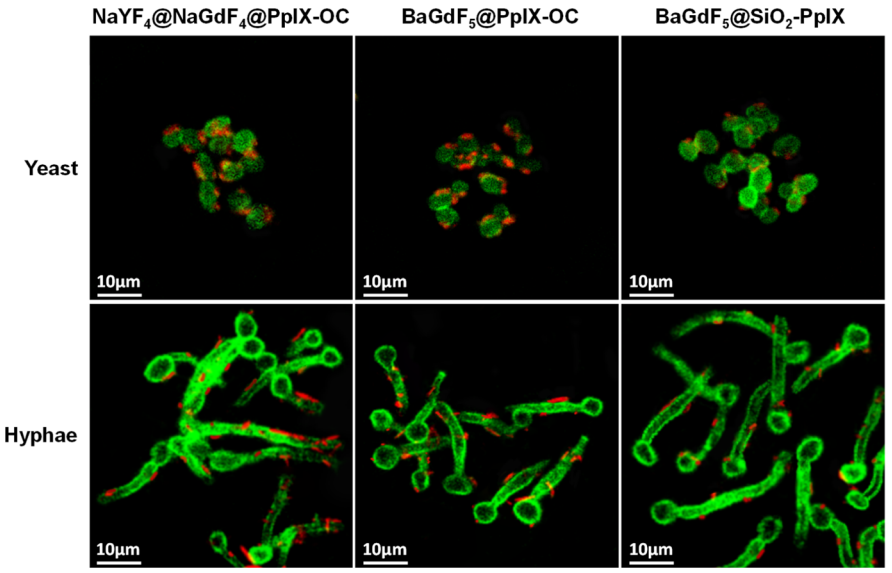

Figure 3. Visualization of the interaction between photodynamic nanoparticles and *Candida albicans* (green: Con A, λex = 488 nm, λem = 505 nm; red: PpIX on the nanoparticles, λex = 524 nm, λem = 630 nm). Scale bars, 10 μm.

SiO_2-PpIX, which was +24.5, +22.5, and +18.2 mV, respectively (as shown in Figure 1h). The positive charge may be favorable for targeting the fungal cells and biofilms by an electrostatic interaction.[29]

The successful loading of PpIX was confirmed by the fluorescence and UV−vis absorption spectra of the photodynamic nanoparticles.[29] The UCNs in this study can be excited by a 980 nm laser to emit green fluorescence with the dominant peak at about 540 nm, as shown in Figure 2a. Meanwhile, $NaYF_4$:Yb,Er@$NaGdF_4$ showed a higher fluorescence than that of $BaGdF_5$:Yb,Er, leading to the difference in the ROS generation efficiency in PDT. The fluorescence intensity was reduced for all the surface-modified nanoparticles, which demonstrated that PpIX was successfully loaded as the fluorescence could be strongly absorbed by PpIX (the absorption spectrum is shown by the gray curve in Figure 2a). Additionally, the UV−vis absorption spectra of the three PDT nanoparticles (Figure 2b) were comparable to that of PpIX, further supporting that PpIX was modified on the nanoparticles. The difference of the fluorescence intensity reduction and the UV−vis absorption intensity between the photodynamic nanoparticles indicated the distinct payload of PpIX for different nanoparticles. Thus, we quantified the payload ratio of PpIX and the corresponding ROS generation. In brief, a standard curve of concentration vs. the UV−vis absorption intensity of PpIX was established, and then, the loading amount of PpIX could be roughly estimated according to the absorption of the nanoparticles.[28,30] The payloads were 38.17, 35.56, and 8.48 wt % for $NaYF_4$@$NaGdF_4$@PpIX-OC, $BaGdF_5$@PpIX-OC, and $BaGdF_5$@SiO_2-PpIX, respectively.

Next, we assessed the ROS production of the nanoparticles by employing 1,3-diphenyl-isobenzofuran (DPBF) as the indicator by recording the quench of its absorption peak at 400 nm, as shown in Figure 2c. Both $NaYF_4$@$NaGdF_4$@PpIX-OC and $BaGdF_5$@PpIX-OC led to over 60% decrease in 10 min. Meanwhile, $BaGdF_5$@SiO_2-PpIX only reduced the absorption of DPBF by about 20%. This result indicated that the ROS production was dependent on the loading amount of PS rather than the fluorescent property of the UCNs. Together, we have prepared three distinct PDT nanoparticles that are different in hydrodynamic size, surface modification, and ROS production, providing the formulations for assessing the impact of these factors on biofilms.

2.2. Inhibition of the Planktonic Fungal Cells by Nanoparticulate PDT. Considering the limited diffusion distance (~10 nm) and the short half-life time (~40 ns) of singlet oxygen, which is the dominant type of ROS in PDT,[10] we first assessed the proximity between the nanoparticles and fungal cells after a 0.5 h incubation. As shown in Figure 3, the cell wall was stained with the fluorescent dye Concanavalin A (Con A),[31] while the red fluorescence reflected the distribution of PpIX loaded onto the nanoparticles. The nanoparticles were found to be closely attached to the cell wall of both yeast and hyphal cells. However, the weak intracellular signals indicated that these three nanoparticles had not been efficiently internalized. Furthermore, more nanoparticles of the two groups modified with OC were attached to the cells than the silica-modified group. This could be explained as follows: the OC embedded into the cell wall enhances the binding efficiency.[32]

The biofilms are highly organized communities developed in four stages: adhesion, proliferation, maturation, and dispersal. The hyphal formation starts after attachment to the external surface, representing the early stage of biofilm formation. Thus, inhibiting the hyphal formation is critical for preventing biofilm formation.[6,7] Therefore, the planktonic yeast cells were induced for filamentation in the Rosewell Park Memorial Institute (RPMI) 1640 culture medium.[33] The micrographs of the cellular morphology change in random fields of vision were shown in 4a; after the PDT with the three different nanoparticles, the hyphal length was much shorter than that of the corresponding control groups without light irradiation, especially within the first 2 h, indicating that PDT could suppress the transition from yeast to hyphae, which was consistent with the investigations based on the PDT using PS molecules. We further used ImageJ software to measure the average hyphal length by randomly selecting about 150 cells from 5 fields in each group and calculated the hyphal inhibitory efficiency by normalizing to the corresponding light-free groups.[34] As shown in Figure 4b, the inhibitory efficiencies

https://doi.org/10.1021/acsomega.2c07740
ACS Omega 2023, 8, 4357−4368

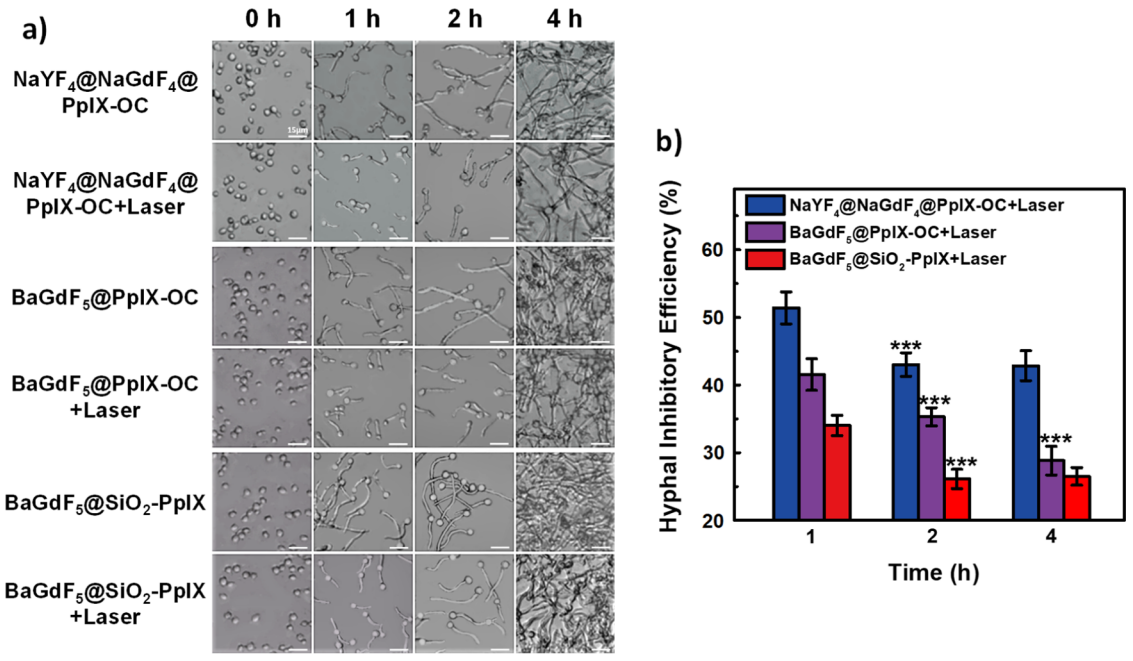

Figure 4. Inhibitory effect on hyphal formation by PDT in 4 h. (a) Microscopy images and (b) inhibition of hyphal growth. The inhibitory efficiency of PDT was calculated by normalizing the hyphal length to the corresponding light-free groups. The values are presented as means ± SD, ***$p < 0.001$.

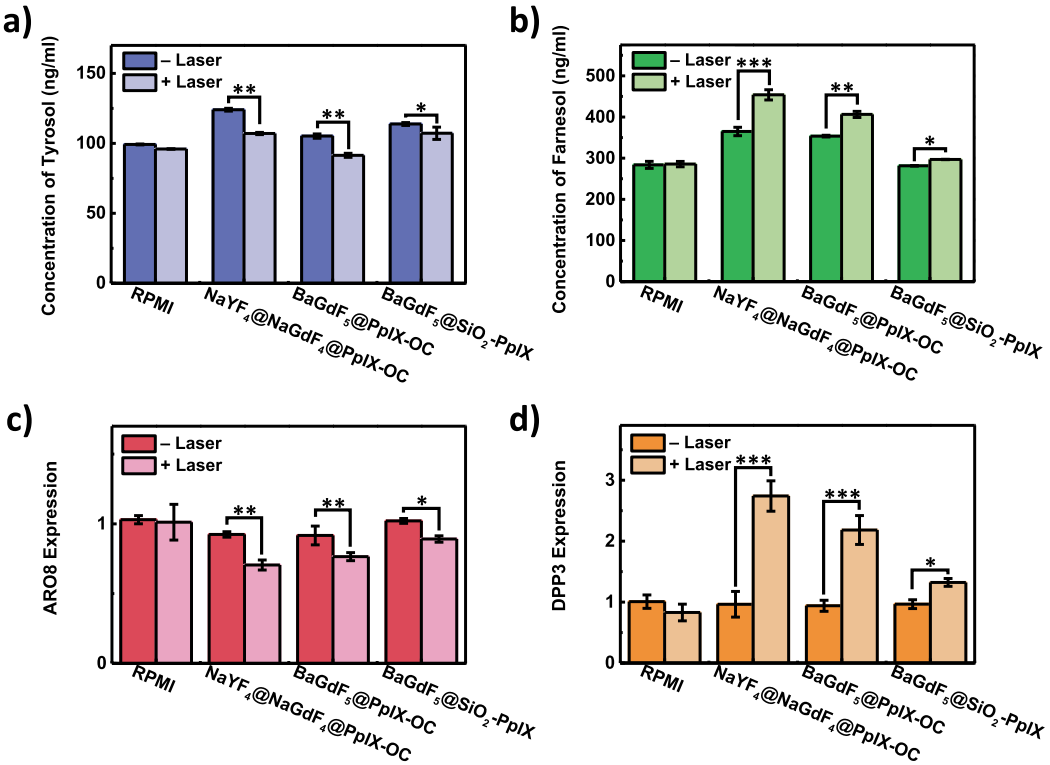

Figure 5. Expressions of (a) tyrosol and (b) farnesol and the transcriptional expression levels of (c) ARO 8 and (d) DPP 3 after applying PDT on planktonic fungi. All the results were compared with those without laser irradiation. The values are presented as means ± SD, *$p < 0.05$, **$p < 0.01$, ***$p < 0.001$.

of PDT were over 40−50% with $NaYF_4$@$NaGdF_4$@PpIX-OC and $BaGdF_5$@PpIX-OC nanoparticles, while $BaGdF_5$@SiO_2-PpIX was the least effective. The highest PDT efficiency of $NaYF_4$@$NaGdF_4$@PpIX-OC nanoparticles might be due to the closest nanoparticle−cell proximity (Figure 3) and the highest ROS production (Figure 2c), resulting in the accumulation of more ROS around the cells. Meanwhile, in the following growing process, there was less difference compared to the light-free groups as the ROS was not generated and the inhibitory effect had faded. Our results indicated that the hyphal transformation was blocked in a local

https://doi.org/10.1021/acsomega.2c07740
ACS Omega 2023, 8, 4357−4368

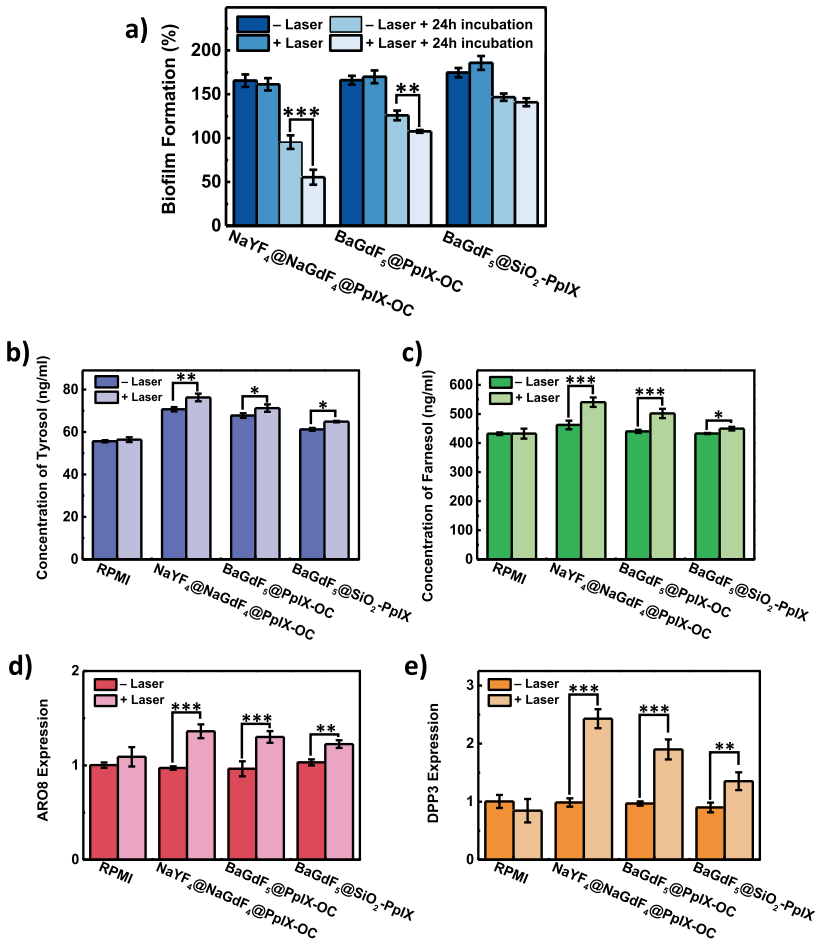

Figure 6. Inhibition of biofilm formation and the expression changes of QS-related molecules and genes by PDT. (a) Inhibition efficiency of biofilm formation with PDT. The biomass was measured immediately after PDT (+Laser) and 21.5 h after PDT (+Laser + 24 h). The comparison groups were measured at the same time points without light irradiation. HPLC quantified the contents of (b) tyrosol and (c) farnesol and the gene expression levels of (d) ARO 8 and (e) DPP 3. The values are presented as means ± SD, $*p < 0.05$, $**p < 0.01$, $***p < 0.001$.

ROS-dependent manner. Thus, PDT could inhibit the formation of biofilms at the stage of hyphae formation.

QS, which is a mechanism of cell−cell communication in microbes, has been recognized as the key factor to determine the hyphal and biofilm formation of *C. albicans*.[24,25] It has been demonstrated that blocking QS can silence bacterial communication, thus preventing the formation of bacterial biofilms or inducing their dispersion.[25] We therefore hypothesized that QS might interfere with PDT.[24,35] For *C. albicans*, farnesol and tyrosol are the typical QS molecules (QSMs), which would be secreted to the extracellular microenvironment and improve (for tyrosol) or inhibit (for farnesol) the hyphal growth and biofilm formation.[36,37] Therefore, we evaluated the expression of QSMs by high-performance liquid chromatography (HPLC).[38] As shown in Figure 5a,b, after the light irradiation, the concentration of tyrosol was reduced. Meanwhile, farnesol was increased for all the three PDT groups in comparison with the control. This result was consistent with the general QSM expression for inhibiting hyphal transformation. We also assessed the expressions of the downstream regulatory genes, DPP 3 and ARO 8, required for farnesol and tyrosol biosynthesis, respectively. DPP 3 encoded phosphatase and was proved to participate in the biosynthesis of farnesol by converting farnesyl pyrophosphate to farnesol,[39] while ARO 8 encoded aromatic aminotransferases I to catalyze the transamination step in the initial stage of tyrosol production and was the first to be activated.[40] Compared to the gene expression levels of ARO 8 and DPP 3 in the control group of RPMI, the expression levels in the test groups of nanoparticles with or without laser treatment were calculated based on the $2^{-\Delta\Delta CT}$ formula. As shown in Figures 5c,d, PDT led to the reduction in ARO 8 expression (for tyrosol) and the increase in DPP 3 expression (for farnesol), both of which were consistent with the alteration of tyrosol and farnesol, respectively. These results indicated that the QSM expressions in *C. albicans* were stimulated by PDT. Moreover, a comparison among the three PDT groups treated with different nanoparticles showed that treatment with $NaYF_4$@$NaGdF_4$@PpIX-OC resulted in the most significant changes of the content of farnesol and tyrosol, which was consistent with the hyphal inhibition results. Thus, PDT might regulate the expression of QSMs to impact the progression of hyphal transformation.

2.3. Suppression of Biofilm Formation by Nanoparticulate PDT. We further tested the efficacy of PDT in suppressing biofilm formation and investigated whether PDT would affect the QS during this process. After 2 h of growth, the biofilm started to be initiated. The nanoparticles were then added to cells with light irradiation applied after a 0.5 h incubation. The fungal cells were left to grow for another 21.5

https://doi.org/10.1021/acsomega.2c07740
ACS Omega 2023, 8, 4357−4368

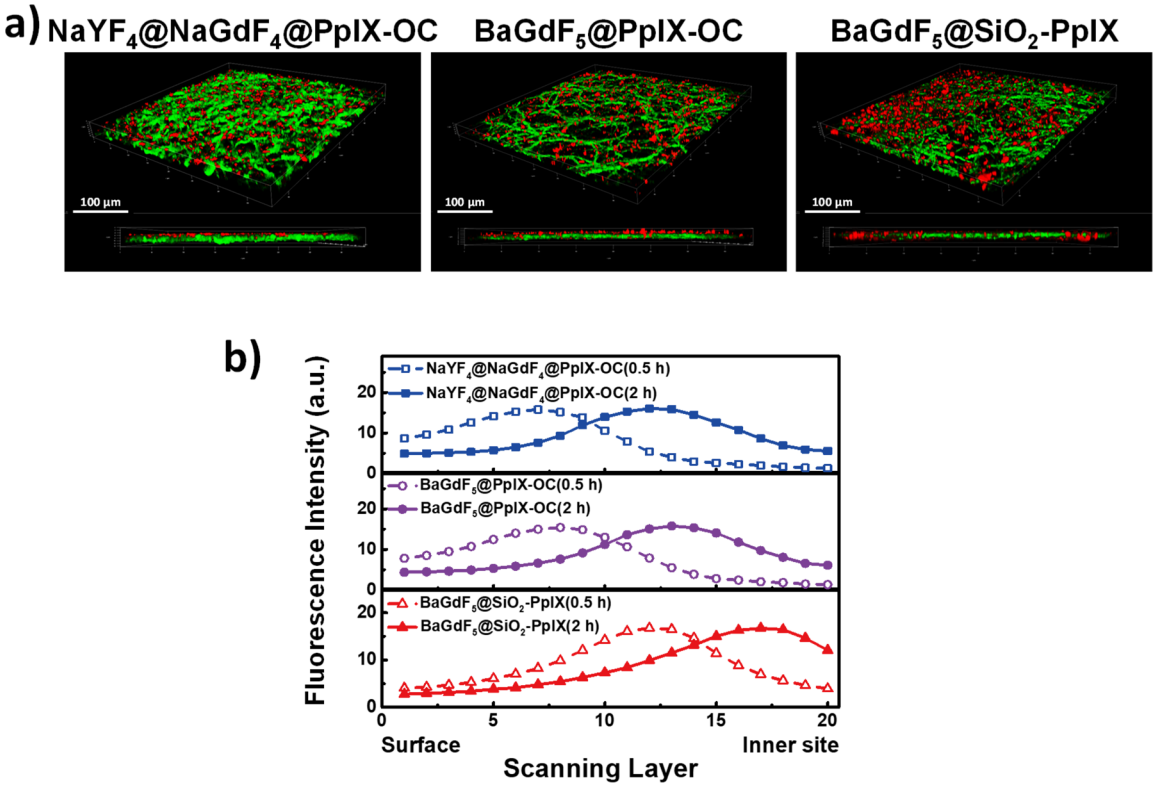

Figure 7. Penetration of nanoparticles in a mature *Candida albicans* biofilm. (a) Confocal fluorescence images after 0.5 h and the (b) relative intensity of PpIX fluorescence in each scanning layer at 0.5 and 2 h when the whole biofilm was observed by laser scanning confocal microscopy in 20 scanning layers from the surface to the inner side. Scale bars, 100 μm.

h to form mature biofilms. The biomass of the biofilm was quantified immediately after light irradiation or after 24 h.[20,41] As shown in Figure 6a, at the early stage of biofilm formation, the biomass in all the three PDT groups was comparable to those in the corresponding non-irradiated control groups. This result indicated that the newly formed biofilm was not directly destroyed at the indicated time point. Interestingly, further incubation led to dramatic biomass reduction not only for the PDT-treated groups but also for the groups in the dark. For those without light, the reduction of biomass was weakened in the order of $NaYF_4$@$NaGdF_4$@PpIX-OC, $BaGdF_5$@PpIX-OC, and $BaGdF_5$@SiO_2-PpIX, which might be attributed to the variance of their surface potentials. Furthermore, applying PDT enhanced the inhibition in the same manner with planktonic cells, which indicated that the inhibition of biofilm formation in the early stage might also require the strong affinity and high ROS production of PDT nanoparticles.

After quantification of the expression level of QSMs right after laser excitation, we found that the concentrations of both tyrosol and farnesol were increased, as shown in Figures 6b,c, which were consistent with the upregulation of ARO 8 (Figure 6d) and DPP 3 (Figure 6e), respectively. Consistent with the biomass results, $NaYF_4$@$NaGdF_4$@PpIX-OC with laser irradiation exhibited the most significant alteration of the content and gene expression of QSMs. Unexpectedly, the expression of tyrosol was opposite to that excreted by planktonic cells. One possible explanation is the self-regulation of the yeast cells within the biofilm, in which tyrosol is secreted during the prometaphase of biofilm formation to promote the hyphal growth and initiate biofilm formation.[24,37] When the microenvironment was disturbed, the secretion of tyrosol would be upregulated to maintain the microbial colony formation. In the meantime, PDT might not directly oxidize tyrosol or hinder the excretion of tyrosol, which is in accordance with previous results that oxidative stress did not change the tyrosol expression.[24]

2.4. Destructing Mature Biofilms by PDT. Mature biofilms consist of both a hyphae-constructed framework and a dense ECM filled in the interspace, which restricts the penetration of antifungal agents.[6,42] Thus, we evaluated the penetration capabilities of the nanoparticles using a laser confocal scanning microscope. Fungal cells were stained with Con A (green fluorescence) to visualize the individual cells within the biofilm, as shown in Figure 7a. For $NaYF_4$@$NaGdF_4$@PpIX-OC, most of the red fluorescence of PpIX was present on the surface of the biofilm, which indicated that the nanoparticles did not infiltrate. Meanwhile, a part of $BaGdF_5$@PpIX-OC penetrated the biofilm with the others detected on the surface. In contrast, most of $BaGdF_5$@SiO_2-PpIX nanoparticles were diffused into the biofilm in 0.5 h, showing the highest penetrating efficiency. The differences of the nanoparticles' penetration could be observed intuitively from the vertical section images of the biofilm (as shown in the lower panel in Figure 7a). We further analyzed the infiltrating speed by quantifying the fluorescence intensity of nanoparticles distributed in each scanning layer. As shown in Figure 7b, at 0.5 h, the nanoparticle layers with a higher fluorescence intensity were closer to the surface of the biofilm, whereas the peak moved inside the biofilms after 2 h. Among the three nanoparticles, $BaGdF_5$@SiO_2-PpIX almost penetrated the biofilm at 0.5 h, while part of the $NaYF_4$@$NaGdF_4$@PpIX-OC and $BaGdF_5$@PpIX-OC nanoparticles remained on the surface and covered only about 50% of the biofilm, showing an obvious variance among the three kinds of nanoparticles. After

https://doi.org/10.1021/acsomega.2c07740
ACS Omega 2023, 8, 4357−4368

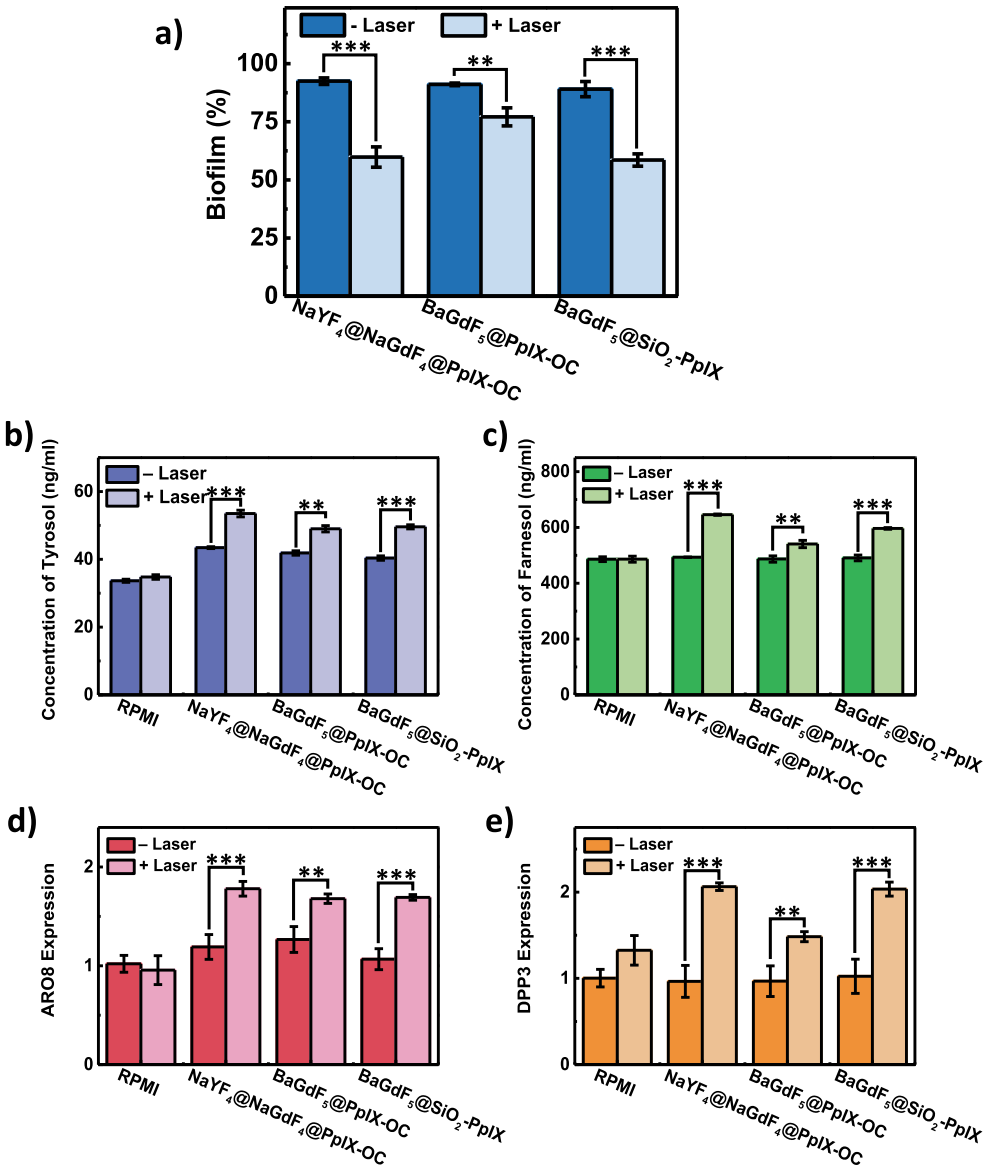

Figure 8. Destruction of a mature biofilm and the upregulation of QS-related molecules and genes by PDT. (a) Relative biomass of the mature biofilm immediately after the PDT with different nanoparticles. The contents of (b) tyrosol and (c) farnesol and the gene expression levels of (d) ARO 8 and (e) DPP 3 after applying PDT on the mature biofilm. The values are presented as means ± SD, $^{**}p < 0.01$, $^{***}p < 0.001$.

2 h, all of the three nanoparticles achieved almost complete infiltration and the difference in biofilm penetration decreased. Notably, the $BaGdF_5$@SiO_2-PpIX nanoparticles with the best penetrating capability had the smallest size. Thus, the penetration capability of positively charged nanoparticles depends on their particle size.

The capability of nanoparticle-based PDT to destruct the mature fungal biofilm was examined. After co-culturing the nanoparticles with the mature biofilm for 0.5 h, a 980 nm laser treatment was applied, and the biofilm biomass was quantified by a 2,3-bis(2-methoxy-4-nitro-5-sulfo-phenyl)-2*H*-tetrazolium-5-carboxanilide (XTT) assay. In contrast to the unaltered biomass immediately after PDT in the biofilm forming stage (Figure 6a), significant biomass reduction was observed in all the PDT groups, as shown in Figure 8a. Although the reason for this diversity is worth further investigation, direct damage of the mature biofilm by PDT could be identified. It was possibly related to the substances excreted in the late stage of biofilm formation that could be decomposed by ROS. Meanwhile, $NaYF_4$@$NaGdF_4$@PpIX-OC and $BaGdF_5$@SiO_2-PpIX induced almost an equal reduction of over 35%, which is higher than that of $BaGdF_5$@ PpIX-OC (about 15%). This result indicated that both ROS generation and penetration are of the same importance. The nanoparticles that efficiently produce ROS can damage the mature biofilm even though they cannot infiltrate. On the contrary, when the nanoparticles approach the target structure closely, the generated ROS could be utilized maximally. We finally measured the content and gene expression of QSMs. As shown in Figure 8b,c, PDT increased the concentration of both tyrosol and farnesol and elevated the expression levels of genes ARO 8 and DPP 3. This result was consistent with that in the early stage of biofilm formation. The upregulation of farnesol at all the stages under PDT indicated that it is positively related with the increased oxidative stress,[35,36,43] leading to the suppression hyphal formation and eventually biofilm formation. Thus, the nanoparticulate PDT can suppress or destruct the forming or formed fungal biofilm. Although efficiency is still needed to be

https://doi.org/10.1021/acsomega.2c07740
ACS Omega 2023, 8, 4357−4368

optimized via enhancing ROS generation and biofilm penetration, our work successfully demonstrated that nanoparticle-based PDT has the potential to inhibit or destruct fungal biofilms.

We showed that sufficient ROS generation of PDT could inhibit the formation of a biofilm and, to some extent, destruct it. Compared with molecular PSs, nanoparticles can concentrate the PS and predictably deliver them to penetrate biofilms. Meanwhile, the nanoparticles that could be stimulated by NIR enabled the application in deep-seated infections. Thus, nanoparticulate PDT might be preventive in places where a fungal biofilm is prone to form. Meanwhile, it might be promising to treat the already formed one. Nonetheless, the destruction efficiency of mature biofilms remained a concern. Eradicating biofilms that have formed is crucial, yet can hardly be achieved in clinics. Our work presented a limited destructing percentage of about 35%. Although the possibility was presented, how to improve the capability of eradication should be considered in the future, which might rely on the development of ROS-producing nanomaterials.

3. EXPERIMENTAL SECTION

3.1. Materials. BaO, Gd_2O_3, Yb_2O_3, Tm_2O_3, and sodium oleate (NaOL, 98%) were purchased from Macklin. 1-Octadecene (ODE, 90%), oleic acid (OA, 90%), APTS, and Igepal CO-520 were purchased from Sigma-Aldrich. Trifluoroacetic acid (TFA, 99.5%) was purchased from Aladdin. Cyclohexane (>99.5%) and anhydrous ethanol (>99.7%) were purchased from Sinopharm Chemical Reagent Co., Ltd.

3.2. Synthesis of $NaYF_4$:20%Yb,0.2%Er@$NaGdF_4$ and $BaGdF_5$:20%Yb,0.2%Er Nanoparticles. $NaYF_4$:20%Yb,0.2%Er@$NaGdF_4$ and $BaGdF_5$:20%Yb,0.2%Er nanoparticles were prepared according to our previous reports.[30,44] First, the precursors, including $(CF_3COO)Na$, $(CF_3COO)_2Ba$, $(CF_3COO)_3Gd$, $(CF_3COO)_3Yb$, and $(CF_3COO)_3Er$, were prepared by dissolving the corresponding metallic oxides in TFA/water (1:1) solutions and stirring with heating at 150 °C till we got clear solutions, and the precursors were collected after drying. Then, for the synthesis of $NaYF_4$:20%Yb,0.2%Er@$NaGdF_4$, the core precursor solution including CF_3COONa (1 mmol), $(CF_3COO)_3Y$ (0.798 mmol), $(CF_3COO)_3Er$ (0.2 mmol), $(CF_3COO)_3Tm$ (0.002 mmol), ODE (2.5 mL), and OA (2.5 mL) and the shell precursor solution including $(CF_3COO)_3Gd$ (1 mmol), sodium oleate (0.63 mmol), ODE (7.5 mL), and OA (7.3 mL) were prepared by stirring at 100 °C under vacuum conditions for 1 h until the mixtures become clear. The reaction solution including sodium oleate (0.63 mmol), ODE (10 mL), and OA (9.8 mL) was heated to 292 °C while being stirred under dry nitrogen before the core precursor was injected into it dropwise. After the injection, the solution was heated to 330 °C quickly and reacted for 10 min. Then, the shell precursor solution was injected and reacted for another 2 min at the end. The final solutions were cooled to room temperature before being washed with chloroform and anhydrous ethanol three times. The collected nanoparticles were dispersed in cyclohexane for further use. For the synthesis of $BaGdF_5$:20%Yb,0.2%Er nanoparticles, the nanoparticle precursor solution including $(CF_3COO)_2Ba$ (1 mmol), $(CF_3COO)_3Gd$ (1 mmol), $(CF_3COO)_3Yb$ (0.2 mmol), $(CF_3COO)_3Tm$ (0.002 mmol), ODE (10 mL), and OA (10 mL) and the reaction solution containing sodium oleate (4 mmol), ODE (15 mL), and OA (14 mL) were heated to 294 °C with stirring under dry nitrogen. After the injection of the precursor solution, the reaction at 330 °C was kept for 30 min.

3.3. Synthesis of $NaYF_4$@$NaGdF_4$@PpIX-OC, $BaGdF_5$@PpIX-OC, and $BaGdF_5$@SiO_2-PpIX. For the PpIX-OC drug loading modification, first, OC and PpIX were conjugated together by EDC-NHS activation as described in our previous study,[28] in which EDC (13.5 mg) and NHS (20 mg) aqueous solution (5 mL) was added into PpIX (10 mg) in DMSO/H_2O (v/v = 1:1, 2 mL) with stirring for 1 h. Then, the OC aqueous solution (10 mg/mL, 1 mL) was added in and stirred for another 12 h. After that, the resultant OC-PpIX solution was added into the chloroform solution dispersed with corresponding nanoparticles (1 mg/mL, 10 mL) and stirred until chloroform was evaporated completely. The final nanoparticles were washed by deionized water three times and re-dispersed in deionized water.

For the SiO_2-PpIX drug loading modification, the APTS-PpIX covalent compound was synthesized following our previous work.[30] Typically, PpIX (100 mg) was activated by oxalyl chloride (3 mL) under a dry nitrogen atmosphere and then, APTS (1 mL) was added for the reaction. The solution was directly used as a silane agent for further modification on the nanoparticles by the procedure in our earlier work.[28]

The morphology and size of the nanoparticles were observed using a 120 kV transmission electron microscope and dynamic light scattering instrument, by which the zeta potential was also measured. The fluorescence spectra were obtained using a Shimadzu RF5301PC luminescence spectrometer with an external laser source of 980 nm.

3.4. Loading Efficiency of PpIX and ROS Generation. The payload was calculated by the weight ratio between PpIX and UCNs and mainly quantified by UV−vis analysis (UV-2550, Shimadzu). A standard calibration curve recording the UV−vis absorbance of PpIX at 535 nm with different concentrations was established at first. Then, absorbance of the nanoparticle aqueous solution at 535 nm was detected, according to which the content of PpIX could be calculated based on the calibration curve because both UCNs and other components show no absorbance at that wavelength. Meanwhile, the amount of UCNs in the solution was detected using an inductively coupled plasma atomic emission spectrometer (iCAP7600, Thermo-Fisher). Then, the weight ratio between PpIX and UCNs was calculated.

After quantifying the concentration of the nanoparticles by an inductively coupled plasma emission spectrometer, the deionized water solution of PpIX-loaded nanoparticles (1 mL) was placed in a 1 mL quartz cuvette, and the UV−vis absorption spectrum was measured. Then, a DPBF acetonitrile solution (20 μL, 8 mM) was added and uniformly mixed. The absorption spectra of the mixture during irradiation were recorded every 2 min using a 980 nm laser (1 W, continuous wave, Xi'An Sapling Institute of Laser Technology). The ROS generation efficiency was evaluated by the reduction of the absorption intensity of DPBF at around 400 nm.

3.5. Strains and Culture Conditions. *C. albicans* strain SC5314 was used in this study and stored at −80 °C. These *C. albicans* strains were recovered on yeast peptone glucose (YPD) medium plates (1% yeast extract, 2% peptone, and 2% glucose) and grown overnight in an incubator at 30 °C. The cells were washed twice using sterile phosphate buffered saline (PBS) and suspended in RPMI 1640 medium (11875093; Gibco). The optical density (OD) of the washed cell

https://doi.org/10.1021/acsomega.2c07740
ACS Omega 2023, 8, 4357−4368

suspensions at 600 nm was measured using a BioTek plate reader.

3.6. Confocal Laser Scanning Microscopy. Yeast cells were cultured in YPD medium at 30 °C for 2 h in the dark, and hyphal cells were cultured in RPMI 1640 medium at 37 °C in the dark for 2 h. The diluted standardized cell suspension (OD600 = 0.05) was inoculated into a 48-well plate with matching cell slides and incubated at 37 °C in the dark for 24 h to form mature biofilms. Following the incubation, the supernatant was aspirated and discarded, and 100 μL of different nanoparticles was added to each well. Then, the plate was incubated in the dark at 37 °C for 30 min. After incubation, each plate in the experimental group was irradiated with a 980 nm laser for 15 min with a laser transmitter. The cells then were cultured at 37 °C in 200 μL of the fluorescent stain Con A (λex = 488 nm, λem = 505 nm) (25 μg/mL) (111072-31-2; Invitrogen) prepared in PBS solution for 45 min. The excess dye was washed using PBS solution, and the cells were fixed with paraformaldehyde for 30 min. The distribution of nanoparticles (λex = 524 nm and λem = 630 nm) around or inside the cells was observed by a confocal laser scanning microscope.

3.7. Filamentation Assay. The standardized cell suspension (OD600 = 0.05) with YPD plus serum medium (10%) and different nanoparticles were seeded in 96-well plates and incubated at 37 °C in the dark for 30 min. After incubation, each plate in the experimental group was irradiated with a 980 nm laser for 15 min. After PDT, the cells were incubated in the dark at 37 °C. The hyphal formation was studied under a microscope at 0, 1, 2, and 4 h, respectively.

3.8. Biofilm Formation. The standardized cell suspension (OD600 = 0.05) was seeded in a 96-well plate and incubated at 37 °C for 2 or 24 h to form biofilms. Following incubation, the supernatant was aspirated and discarded, and 100 μL of different nanoparticles was added to each well. Then, the plate was incubated in the dark at 37 °C for 30 min. After incubation, each plate in the experimental group was irradiated with a 980 nm laser for 15 min. The biofilm formation was measured by a XTT reduction assay. XTT (111072-31-2; Invitrogen) was prepared at a concentration of 1 mg/mL in PBS solution, and menadione was prepared at 0.4 mM in acetone. Prior to each assay, a 100 μL aliquot of XTT/menadione (200 μg/mL XTT and 4 μM menadione) solution was prepared and added to each prewashed biofilm to measure the biofilm formation. The plate was then incubated at 37 °C in the dark for 4 h. After incubation, the liquid was removed from each well and transferred to a new 96-well plate, and formazan production was measured by determining the absorbance at 492 nm using a fluorescent microplate reader.

3.9. High-Performance Liquid Chromatography. The standardized cell suspension (OD600 = 0.05) with different nanocarriers was inoculated into 96-well multiple-well plates. In order to avoid the volatilization loss of farnesol, the cell suspension was covered with a 15% volume of decane to collect farnesol. The plate was incubated at 37 °C in the dark for 30 min. After incubation, each plate in the experimental group was irradiated at 980 nm for 15 min. After PDT, the upper decane phase was collected for farnesol extraction. The supernatant was centrifuged at 10,000*g* for 15 min and then filtered with a 0.22 μm membrane to separate tyrosol. The concentrations of farnesol and tyrosol were quantified by HPLC.

3.10. Quantitative Real-Time PCR. The photodynamic-treated cells were collected by centrifugation, and total RNA was extracted using a Direct-zol RNA Miniprep kit (R2072-50; ZYMO RESEARCH). The RT reagent kit (RR047A; Takara) was used to transcribe total RNA into the cDNA. The RT-PCR analysis was performed using the Bimake-2x-SYBR-Green qPCR Master Mix Kit (B21202; Bimake) according to the manufacturer's instructions. The nucleotide sequences of all primers were as shown below: ADH1 forward: TGACGGTGGTGACGAAAAAG, reverse: TGTGGACCAC-CATCAGTAGC; ADH2 forward: TGCTGAAC-CAAACTGTGCTG, reverse: TGCAACATTGGC-TAAGTCGG; ADH3 forward: TTGACTCCATTCCATGC-CATTC, reverse: CAGAAGCAACAATGTGACAACC; ADH5 forward: TAACAAGCCAGGTGCTGGTC, reverse: CAGCAATTTCGTGGCCCATC; ARO8 forward: TTAGC-CAATGCGTTGTTGCG, reverse: GGAACAAACTGGTC-CAAGGC; ARO9 forward: AAACCAAAACTCCGCCTTCC, reverse: GGTGCATGACCTTCAACAGC; ARO10 forward: CAGCACAAATGACGGTGCAA, reverse: AGACC-GATTTGGGCCTTTGA; DPP3 forward: ATACTTGGGTTTCAAGCATTGG, reverse: TGGGAG-TATCATTTGCTGGTTG; ACT1 forward: TTGTTGACC-GAAGCTCCAATG, reverse: CCGGTGGTTCTACCAGAA-GAG.

4. CONCLUSIONS

In this study, we introduced a nanoparticulate PDT method and evaluated its potential in suppressing early- and late-stage biofilm formation. Specifically, we have designed three PDT nanoparticles with different ROS-generating efficiencies, surface compositions, and hydrodynamic sizes. We found that the OC-modified nanoparticles have a better affinity to yeast and hyphal cells than the silane-modified ones, which resulted in a higher efficiency in inhibiting the yeast−hyphae transition after exposure to the laser. Nanoparticles modified with OC led to a better suppressing effect in the early stage of biofilm formation. Thus, ROS generation and the binding affinity to planktonic cells should be the pivotal factors for inhibiting the initiation of biofilms. In contrast, a mature fungal biofilm limited the penetration by the size of the nanoparticles. We discovered that the 15 nm $BaGdF_5$@SiO_2-PpIX nanoparticles penetrated deep inside the biofilm, which dramatically improved the destruction efficiency to the level that was comparable to the biggest nanoparticle with the highest ROS production ($NaYF_4$@$NaGdF_4$@PpIX-OC). These results indicated that complete penetration and sufficient ROS generation could be necessary to eliminate mature biofilms. Therefore, the requirements of nanoparticles, PS, and surface modification for biofilms and fungal cells were different. Since the surface could be modified with the target molecules, the size could be adjusted, and the capability of ROS generation could be optimized; nanoparticle-based PDT might be superior in combating fungal biofilms compared to PS molecules.

AUTHOR INFORMATION

Corresponding Authors

Ning-Ning Liu − *State Key Laboratory of Oncogenes and Related Genes, Center for Single-Cell Omics, School of Public Health, Shanghai Jiao Tong University School of Medicine, Shanghai 200025, China*; Email: liuningning@sibcb.ac.cn

Ke Tao − *State Key Lab of Metal Matrix Composites, School of Materials Science and Engineering, Shanghai Jiao Tong*

https://doi.org/10.1021/acsomega.2c07740
ACS Omega 2023, 8, 4357−4368

University, Shanghai 200240, P. R. China; orcid.org/0000-0002-8014-8587; Email: ktao@sjtu.edu.cn

Authors

Na Tang − *State Key Lab of Metal Matrix Composites, School of Materials Science and Engineering, Shanghai Jiao Tong University, Shanghai 200240, P. R. China;* orcid.org/0000-0001-8798-218X

Shenghao Yuan − *State Key Laboratory of Oncogenes and Related Genes, Center for Single-Cell Omics, School of Public Health, Shanghai Jiao Tong University School of Medicine, Shanghai 200025, China*

Yuxuan Luo − *State Key Laboratory of Oncogenes and Related Genes, Center for Single-Cell Omics, School of Public Health, Shanghai Jiao Tong University School of Medicine, Shanghai 200025, China*

An-Jun Wang − *State Key Laboratory of Oncogenes and Related Genes, Center for Single-Cell Omics, School of Public Health, Shanghai Jiao Tong University School of Medicine, Shanghai 200025, China*

Kang Sun − *State Key Lab of Metal Matrix Composites, School of Materials Science and Engineering, Shanghai Jiao Tong University, Shanghai 200240, P. R. China*

Complete contact information is available at: https://pubs.acs.org/10.1021/acsomega.2c07740

Author Contributions

§N.T., S.Y., and Y.L. are co-first authors.

Notes

The authors declare no competing financial interest.

■ ACKNOWLEDGMENTS

This work was financially supported by the National Key R&D Program of China (2020YFA0907200) and the National Natural Science Foundation of China (31900129, 31671004 and 31671027). We thank the Instrumental Analysis Center of Shanghai Jiao Tong University for assistance with the instrumentation. We thank X. C. Zhu from the Core Facility of Basic Medical Sciences at Shanghai Jiao Tong University School of Medicine for the assistance during the LC−MS/MS data collection.

■ REFERENCES

(1) Bongomin, F.; Gago, S.; Oladele, R. O.; Denning, D. W. Global and Multi-National Prevalence of Fungal Diseases-Estimate Precision. *J. Fungi* **2017**, *3*, 57.

(2) (a) Hosseini-Moghaddam, S. M.; Ouédraogo, A.; Naylor, K. L.; Bota, S. E.; Husain, S.; Nash, D. M.; Paterson, J. M. Incidence and outcomes of invasive fungal infection among solid organ transplant recipients: A population-based cohort study. *Transplant Infect. Dis.* **2020**, *22*, No. e13250. (b) Nganthavee, V.; Phutthasakda, W.; Atipas, K.; Tanpong, S.; Pungprasert, T.; Dhirachaikulpanich, D.; Krithin, S.; Tanglitanon, S.; Jutidamrongphan, W.; Owattanapanich, W.; Chayakulkeeree, M.; Phikulsod, P. Correction to: High incidence of invasive fungal infection during acute myeloid leukemia treatment in a resource-limited country: clinical risk factors and treatment outcomes. *Support. Care Cancer* **2019**, *27*, 3623.

(3) Patel, M. H.; Patel, R. D.; Vanikar, A. V.; Kanodia, K. V.; Suthar, K. S.; Nigam, L. K.; Patel, H. V.; Patel, A. H.; Kute, V. B.; Trivedi, H. L. Invasive fungal infections in renal transplant patients: a single center study. *Renal Failure* **2017**, *39*, 294−298.

(4) (a) Andes, D. R.; Safdar, N.; Baddley, J. W.; Playford, G.; Reboli, A. C.; Rex, J. H.; Sobel, J. D.; Pappas, P. G.; Kullberg, B. J.; Grp, M. S. Impact of Treatment Strategy on Outcomes in Patients with Candidemia and Other Forms of Invasive Candidiasis: A Patient-Level Quantitative Review of Randomized Trials. *Clin. Infect. Dis.* **2012**, *54*, 1110−1122. (b) Mermel, L. A.; Allon, M.; Bouza, E.; Craven, D. E.; Flynn, P.; O'Grady, N. P.; Raad, I. I.; Rijnders, B. J. A.; Sherertz, R. J.; Warren, D. K. Clinical Practice Guidelines for the Diagnosis and Management of Intravascular Catheter-Related Infection: Update by the Infectious Diseases Society of America. *Clin. Infect. Dis.* **2009**, *49*, 1−45.

(5) Nobile, C. J.; Johnson, A. D. Candida albicans Biofilms and Human Disease. *Annu. Rev. Microbiol.* **2015**, *69*, 71−92.

(6) Atriwal, T.; Azeem, K.; Husain, F. M.; Hussain, A.; Khan, M. N.; Alajmi, M. F.; Abid, M. Mechanistic Understanding of Candida albicans Biofilm Formation and Approaches for Its Inhibition. *Front. Microbiol.* **2021**, *12*, 638609.

(7) Chong, P. P.; Chin, V. K.; Wong, W. F.; Madhavan, P.; Yong, V. C.; Looi, C. Y. Transcriptomic and Genomic Approaches for Unravelling Candida albicans Biofilm Formation and Drug Resistance-An Update. *Genes* **2018**, *9*, 540.

(8) (a) Alonso, B.; Pérez-Granda, M. J.; Rodríguez-Huerta, A.; Rodríguez, C.; Bouza, E.; Guembe, M. The optimal ethanol lock therapy regimen for treatment of biofilm-associated catheter infections: an in-vitro study. *J. Hosp. Infect.* **2018**, *100*, e187−e195. (b) Carratalà, J. The antibiotic-lock technique for therapy of 'highly needed' infected catheters. *Clin. Microbiol. Infect.* **2002**, *8*, 282−289.

(9) Pérez-Sáez, M. J.; Mir, M.; Montero, M. M.; Crespo, M.; Montero, N.; Gómez, J.; Horcajada, J. P.; Pascual, J. Invasive Aspergillosis in Kidney Transplant Recipients: A Cohort Study. *Exp. Clin. Transplant* **2014**, *12*, 101−105.

(10) Gunaydin, G.; Gedik, M. E.; Ayan, S. Photodynamic Therapy for the Treatment and Diagnosis of Cancer-A Review of the Current Clinical Status. *Front. Chem.* **2021**, *9*, 686303.

(11) Youf, R.; Müller, M.; Balasini, A.; Thétiot, F.; Müller, M.; Hascoët, A.; Jonas, U.; Schönherr, H.; Lemercier, G.; Montier, T.; Le Gall, T. Antimicrobial Photodynamic Therapy: Latest Developments with a Focus on Combinatory Strategies. *Pharmaceutics* **2021**, *13*, 1995.

(12) Duguay, B. A.; Herod, A.; Pringle, E. S.; Monro, S. M. A.; Hetu, M.; Cameron, C. G.; McFarland, S. A.; McCormick, C. Photodynamic Inactivation of Human Coronaviruses. *Viruses* **2022**, *14*, 110.

(13) (a) Dosselli, R.; Millioni, R.; Puricelli, L.; Tessari, P.; Arrigoni, G.; Franchin, C.; Segalla, A.; Teardo, E.; Reddi, E. Molecular targets of antimicrobial photodynamic therapy identified by a proteomic approach. *J. Proteomics* **2012**, *77*, 329−343. (b) Hu, X.; Huang, Y. Y.; Wang, Y.; Wang, X.; Hamblin, M. R. Antimicrobial Photodynamic Therapy to Control Clinically Relevant Biofilm Infections. *Front. Microbiol.* **2018**, *9*, 1299. (c) Lam, M.; Jou, P. C.; Lattif, A. A.; Lee, Y.; Malbasa, C. L.; Mukherjee, P. K.; Oleinick, N. L.; Ghannoum, M. A.; Cooper, K. D.; Baron, E. D. Photodynamic Therapy with PPcc 4 Induces Apoptosis of Candida albicans. *Photochem. Photobiol.* **2011**, *87*, 904−909. (d) Lopes, D.; Melo, T.; Santos, N.; Rosa, L.; Alves, E.; Clara Gomes, M. C.; Cunha, A.; Neves, M. G. P. M. S.; Faustino, M. A. F.; Domingues, M. R. M.; Almeida, A. Evaluation of the interplay among the charge of porphyrinic photosensitizers, lipid oxidation and photoinactivation efficiency in Escherichia coli. *J. Photochem. Photobiol., B* **2014**, *141*, 145−153.

(14) Černáková, L.; Light, C.; Salehi, B.; Rogel-Castillo, C.; Victoriano, M.; Martorell, M.; Sharifi-Rad, J.; Martins, N.; Rodrigues, C. F. Novel Therapies for Biofilm-Based Candida spp. Infections. *Adv. Exp. Med. Biol.* **2019**, *1214*, 93−123.

(15) Rosseti, I. B.; Chagas, L. R.; Costa, M. S. Photodynamic antimicrobial chemotherapy (PACT) inhibits biofilm formation by Candida albicans, increasing both ROS production and membrane permeability. *Laser Med. Sci.* **2014**, *29*, 1059−1064.

(16) Černáková, L.; Chupáčová, J.; Židlíková, K.; Bujdáková, H. Effectiveness of the Photoactive Dye Methylene Blue versus Caspofungin on the Candida parapsilosis Biofilm invitro and exvivo. *Photochem. Photobiol.* **2015**, *91*, 1181−1190.

(17) Costa, A. C. B. P.; Rasteiro, V. M. C.; Pereira, C. A.; Rossoni, R. D.; Junqueira, J. C.; Jorge, A. O. C. The effects of rose bengal- and

erythrosine-mediated photodynamic therapy on Candida albicans. *Mycoses* **2012**, *55*, 56−63.
(18) Dai, T. H.; Fuchs, B. B.; Coleman, J. J.; Prates, R. A.; Astrakas, C.; St Denis, T. G.; Ribeiro, M. S.; Mylonakis, E.; Hamblin, M. R.; Tegos, G. P. Concepts and principles of photodynamic therapy as an alternative antifungal discovery platform. *Front. Microbiol.* **2012**, *3*, 120.
(19) (a) Calixto, G. M. F.; de Annunzio, S. R.; Victorelli, F. D.; Frade, M. L.; Ferreira, P. S.; Chorilli, M.; Fontana, C. R. Chitosan-Based Drug Delivery Systems for Optimization of Photodynamic Therapy: a Review. *AAPS PharmSciTech* **2019**, *20*, 253. (b) Ziental, D.; Mlynarczyk, D. T.; Czarczynska-Goslinska, B.; Lewandowski, K.; Sobotta, L. Photosensitizers Mediated Photodynamic Inactivation against Fungi. *Nanomaterials* **2021**, *11*, 2883.
(20) Ma, J.; Shi, H.; Sun, H. Y.; Li, J. Y.; Bai, Y. Antifungal effect of photodynamic therapy mediated by curcumin on Candida albicans biofilms in vitro. *Photodiagn. Photodyn. Ther.* **2019**, *27*, 280−287.
(21) (a) Gunaydin, G.; Gedik, M. E.; Ayan, S. Photodynamic Therapy-Current Limitations and Novel Approaches. *Front. Chem.* **2021**, *9*, 691697. (b) Yan, K.; Zhang, Y. B.; Mu, C. L.; Xu, Q. N.; Jing, X. A.; Wang, D. Q.; Dang, D. F.; Meng, L. J.; Ma, J. Z. Versatile Nanoplatforms with enhanced Photodynamic Therapy: Designs and Applications. *Theranostics* **2020**, *10*, 7287−7318.
(22) Songca, S. P.; Adjei, Y. Applications of Antimicrobial Photodynamic Therapy against Bacterial Biofilms. *Int. J. Mol. Sci.* **2022**, *23*, 3209.
(23) Cavalheiro, M.; Teixeira, M. C. Candida Biofilms: Threats, Challenges, and Promising Strategies. *Front. Med.* **2018**, *5*, 28.
(24) Tian, X. Y.; Ding, H.; Ke, W. X.; Wang, L. Q. Quorum Sensing in Fungal Species. *Annu. Rev. Microbiol.* **2021**, *75*, 449−469.
(25) Warrier, A.; Satyamoorthy, K.; Murali, T. S. Quorum-sensing regulation of virulence factors in bacterial biofilm. *Future Microbiol.* **2021**, *16*, 1003−1021.
(26) Forier, K.; Messiaen, A. S.; Raemdonck, K.; Nelis, H.; De Smedt, S.; Demeester, J.; Coenye, T.; Braeckmans, K. Probing the size limit for nanomedicine penetration into Burkholderia multivorans and Pseudomonas aeruginosa biofilms. *J. Controlled Release* **2014**, *195*, 21−28.
(27) (a) Hamblin, M. R. Upconversion in photodynamic therapy: plumbing the depths. *Dalton Trans.* **2018**, *47*, 8571−8580. (b) Li, H.; Wang, X.; Huang, D.; Chen, G. Recent advances of lanthanide-doped upconversion nanoparticles for biological applications. *Nanotechnology* **2020**, *31*, 072001. (c) Zhang, Y. X.; Huang, P.; Wang, D.; Chen, J. C.; Liu, W. Z.; Hu, P.; Huang, M. D.; Chen, X. Y.; Chen, Z. Near-infrared-triggered antibacterial and antifungal photodynamic therapy based on lanthanide-doped upconversion nanoparticles. *Nanoscale* **2018**, *10*, 15485−15495.
(28) Chen, D.; Tao, R.; Tao, K.; Chen, B.; Choi, S. K.; Tian, Q.; Xu, Y.; Zhou, G.; Sun, K. Efficacy Dependence of Photodynamic Therapy Mediated by Upconversion Nanoparticles: Subcellular Positioning and Irradiation Productivity. *Small* **2017**, *13*, 1602053.
(29) Nag, M.; Lahiri, D.; Mukherjee, D.; Banerjee, R.; Garai, S.; Sarkar, T.; Ghosh, S.; Dey, A.; Ghosh, S.; Pattnaik, S.; Edinur, H. A.; Kari, Z. A.; Pati, S.; Ray, R. R. Functionalized Chitosan Nanomaterials: A Jammer for Quorum Sensing. *Polymers* **2021**, *13*, 2533.
(30) Liu, Y.; Xu, Y. W.; Zhang, Z. Z.; Huo, Y. Y.; Chen, D. X.; Ma, W.; Sun, K.; Tonga, G. Y.; Zhou, G. D.; Kohane, D. S.; Tao, K. A Simple, Yet Multifunctional, Nanoformulation for Eradicating Tumors and Preventing Recurrence with Safely Low Administration Dose. *Nano Lett.* **2019**, *19*, 5515−5523.
(31) Tenório, D. P. L. A.; Andrade, C. G.; Cabral Filho, P. E.; Sabino, C. P.; Kato, I. T.; Carvalho, L. B.; Alves, S.; Ribeiro, M. S.; Fontes, A.; Santos, B. S. CdTe quantum dots conjugated to concanavalin A as potential fluorescent molecular probes for saccharides detection in Candida albicans. *J. Photochem. Photobiol., B* **2015**, *142*, 237−243.
(32) Verlee, A.; Mincke, S.; Stevens, C. V. Recent developments in antibacterial and antifungal chitosan and its derivatives. *Carbohydr. Polym.* **2017**, *164*, 268−283.
(33) Holtappels, M.; Swinnen, E.; De Groef, L.; Wuyts, J.; Moons, L.; Lagrou, K.; Van Dijck, P.; Kucharíková, S. Antifungal Activity of Oleylphosphocholine on In Vitro and In Vivo Candida albicans Biofilms. *Antimicrob. Agents Chemother.* **2018**, *62*, No. e01767-17.
(34) Mao, X.; Yang, L.; Fan, Y.; Wang, J.; Cui, D.; Yu, D.; Yu, Q.; Li, M. The Vacuole and Mitochondria Patch (vCLAMP) Protein Mcp1 Is Involved in Maintenance of Mitochondrial Function and Mitophagy in Candida albicans. *Front. Microbiol.* **2021**, *12*, 633380.
(35) Wongsuk, T.; Pumeesat, P.; Luplertlop, N. Fungal quorum sensing molecules: Role in fungal morphogenesis and pathogenicity. *J. Basic Microbiol.* **2016**, *56*, 440−447.
(36) Kovács, R.; Majoros, L. Fungal Quorum-Sensing Molecules: A Review of Their Antifungal Effect against Candida Biofilms. *J. Fungi* **2020**, *6*, 99.
(37) Rodrigues, C. F.; Černáková, L. Farnesol and Tyrosol: Secondary Metabolites with a Crucial quorum-sensing Role in Candida Biofilm Development. *Genes* **2020**, *11*, 444.
(38) Pilařová, V.; Kočová Vlčková, H.; Jung, O. N.; Protti, M.; Buchta, V.; Mercolini, L.; Svec, F.; Nováková, L. Unambiguous determination of farnesol and tyrosol in vaginal fluid using fast and sensitive UHPLC-MS/MS method. *Anal. Bioanal. Chem.* **2020**, *412*, 6529−6541.
(39) (a) Costa, A. F.; Silva, L. D.; Amaral, A. C. Farnesol: An approach on biofilms and nanotechnology. *Med. Mycol.* **2021**, *59*, 958−969. (b) Zhang, L.; Chang, W.; Sun, B.; Groh, M.; Speicher, A.; Lou, H. Bisbibenzyls, a New Type of Antifungal Agent, Inhibit Morphogenesis Switch and Biofilm Formation through Upregulation of DPP3 in Candida albicans. *PLoS One* **2011**, *6*, No. e28953.
(40) Avbelj, M.; Zupan, J.; Raspor, P. Quorum-sensing in yeast and its potential in wine making. *Appl. Microbiol. Biotechnol.* **2016**, *100*, 7841−7852.
(41) Sherwani, M. A.; Tufail, S.; Khan, A. A.; Owais, M. Gold Nanoparticle-Photosensitizer Conjugate Based Photodynamic Inactivation of Biofilm Producing Cells: Potential for Treatment of C. albicans Infection in BALB/c Mice. *PLoS One* **2015**, *10*, No. e0131684.
(42) Bonhomme, J.; d'Enfert, C. Candida albicans biofilms: building a heterogeneous, drug-tolerant environment. *Curr. Opin. Microbiol.* **2013**, *16*, 398−403.
(43) Mehmood, A.; Liu, G.; Wang, X.; Meng, G.; Wang, C.; Liu, Y. Fungal Quorum-Sensing Molecules and Inhibitors with Potential Antifungal Activity: A Review. *Molecules* **2019**, *24*, 1950.
(44) Tang, N.; Wang, X. Y.; Zhu, J.; Sun, K.; Li, S. T.; Tao, K. Labelling stem cells with a nanoprobe for evaluating the homing behaviour in facial nerve injury repair. *Biomater Sci-Uk* **2022**, *10*, 808−818.

https://doi.org/10.1021/acsomega.2c07740
ACS Omega 2023, 8, 4357−4368